X-ray diffraction analysis and microstructures of laser powder bed fusion Ti6Al4V for application in aerospace structural components

Diali Phillip Mokoena[1*], *Thywill* Dzogbewu[1], *Amos* Muiruri[1, 2] and *Deon* de Beer[1]

[1*] Department of Mechanical and Mechatronics Engineering, Central University of Technology, Free State, South Africa
[1, 2] Department of Mechanical Engineering, Murang'a University of Technology, Murang'a, Kenya,

Abstract. X-ray diffraction (XRD) is a powerful tool for analysing crystallographic structure and phase composition of materials. A metastable martensitic α'-phase is formed because of the laser powder bed fusion's (LPBF) rapid cooling rates, whilst a balanced mixture of α and β phases for this material can be obtained upon post process heat treatment. XRD analysis provides insights into the volume fraction of α'-phase transformations upon post-processing at different temperatures. This paper explores the XRD-based phase identification of LPBF processed Ti6Al4V, emphasizing the effects of heat treatments on microstructural evolution. The as-built microstructure primarily consisted of fine acicular α' martensite. Post-processing heat treatments, such as stress-relieving and annealing facilitated the transformation of α' into a stable α + β microstructure. Following annealing, the acicular α′ martensitic microstructure of LPBF Ti-6Al-4V decomposes into a stable lamellar α+β microstructure. The resulting lamellar morphology consisted of alternating α and β laths within prior β grains.

1 Introduction

The aerospace industry is increasingly relying on additive manufacturing (AM) technology to fabricate complex and lightweight structural components with high-performance materials like Ti6Al4V extra-low interstitial (ELI) [1, 2]. The alloy has long held a prestigious position within the aerospace industry owing to its excellent combination of high specific strength, corrosion resistance, and fatigue performance [2, 3].

Corresponding author: mokoenaphillipdgmail.com

The development and application of Ti6Al4V in the aerospace field is driven by the need to balance structural efficiency with operational reliability. This alloy comprises of 6% aluminium, 4% vanadium and 90% titanium, and usually exhibits a unique two phase (α+β) microstructure. Aluminium acts as an α-phase stabilizer, promoting high temperature strength and low density, while vanadium stabilizes the β-phase, improving toughness and ductility [4]. The α and β phases are stable at room temperature.

Traditional manufacturing routes such as forging, casting, and machining, though long established and effective, impose limitations on achievable geometries and material utilization [4]. Machining titanium alloys into complex aerospace components often generates significant waste, while their high reactivity at elevated temperatures necessitates strict atmospheric control, further increasing production costs. In contrast, laser powder bed fusion (LPBF) additive manufacturing overcomes many of these limitations by enabling the fabrication of near-net-shape components with intricate geometries that are difficult or impossible to achieve via conventional methods. LPBF also minimizes material waste, reduces the buy-to-fly ratio, and allows for controlled microstructures through process parameter optimization and post-build heat treatments. These capabilities make LPBF particularly attractive for producing lightweight, high-performance structural components in aerospace applications, where both geometric complexity and material efficiency are critical. The complex geometries produced via LPBF include optimized structures with internal channels, lattices, and undercut features [5].

Nevertheless, the mechanical performance of LPBF parts is heavily influenced by the resulting microstructure, which can differ from wrought counterparts [6]. Consequently, extensive post-processing and detailed characterization are required before such parts can be qualified for critical aerospace use [6, 7]. These attributes are indispensable in the development of structural components where weight savings, mechanical integrity, and durability are critical. In the quest for enhanced performance and efficiency, aerospace engineers continuously seek innovative manufacturing technologies capable of producing intricate geometries without compromising material properties [9]. However, the LPBF process induces unique microstructural characteristics that significantly influence the material's mechanical behaviour [10, 11]. A comprehensive understanding of these microstructural features and phase transformations is critical for optimizing the performance of LPBF-produced Ti6Al4V components [12, 13]. In the LPBF process, thin melted layers are stacked layer by layer as a high energy laser beam selectively scans a metal powder to create a three-dimensional (3D) object. The high heat input and limited volume of the melt pool enables rapid cooling ($>10^3$ K s^{-1}) [14, 15].

The manufactured layers repeatedly melt and solidify throughout the production process. Micro-residual stresses and strain are created in the manufactured parts when the produced layers restrict the contraction with the current layer [16]. Initiation of cracks may result from residual stresses, which will ultimately shorten parts' fatigue lifetime [17]. To lessen the remaining residual stresses created in the printed parts, post-processing techniques such as thermal stress relieving are introduced to LPBF parts [17, 18, 6]. Furthermore, rapid cooling inherent in LPBF results in the formation of a needle-like microstructure commonly referred to as alu. This type of microstructure is formed as a results of cooling rates that ranges from 10^3-10^6 K/s, for Ti6Al4V alloy from temperature in the β-field that are higher during the LPBF process [19, 20]. The acicular α′ martensitic microstructure is inherently brittle and therefore undesirable for demanding structural applications. To overcome these limitations, high-temperature heat treatment is applied to decompose the α′ martensite into a stable two-

phase microstructure consisting of equilibrium α and β phases. This transformation not only relieves residual stresses generated during rapid solidification but also enhances the optimal strength and ductility. Consequently, the annealed α+β microstructure provides improved mechanical stability and damage tolerance, making it far more suitable for aerospace and other high-performance engineering applications [19]. The increase in thermal energy at elevated temperatures enhances atomic mobility, enabling atoms to migrate across grain boundaries. This process reduces the system's overall free energy by overcoming the boundary energy barrier, which in turn promotes grain boundary migration and grain growth. [20, 21]. As a result, Ti6Al4V (ELI) grain coarsening occurs at higher annealing temperatures. However, excessive coarsening diminishes the strengthening effect associated with grain boundary density (Hall–Petch relationship), which can lead to a reduction in yield strength and fatigue resistance. Although larger grains may improve ductility by facilitating easier dislocation motion, the trade-off often results in compromised mechanical performance, particularly in applications such as aerospace where both strength and fatigue resistance are critical. Ti6Al4V alloy is widely used in structural applications at room temperature and in the intermediate service temperature range of approximately 250–400 °C, where it maintains an excellent balance of strength, toughness, and corrosion resistance. This temperature window covers many aerospace and biomedical applications, as higher service temperatures can lead to microstructural instability, phase transformations, and a consequent reduction in mechanical performance. Zhao *et al.* [24] reported that the application of Ti6Al4V above 400°C can affect the microstructures. Song *et al*, 16, reported that the microstructure of LPBF built samples has minimal sensitivity to temperatures below 500°C, with changes only occurring above this temperature leading to decomposition of α′ martensite into equilibrium α + β phases. The difference in the two studies is the soaking time. Zhao *et al*. [22], soaked samples for four hours while Song *et al*. [23], soaked samples for 30 minutes [14]. Various microstructures are found in Ti6Al4V alloy such as lamellae, equiaxed, martensitic, bimodal, and Widmanstätten. Lamellae microstructure has good creep and high fatigue crack growth resistance, while equiaxed has high fatigue crack initiation resistance. The bimodal microstructure in Ti6Al4V alloys arises from a mixture of equiaxed primary α grains and transformed lamellar α+β colonies. This morphology is often tailored through thermo-mechanical or heat treatments to achieve a balance mechanical properties of strength and ductility. The equiaxed α grains contribute to enhanced ductility and fatigue resistance by impeding crack initiation and promoting uniform plastic deformation. In contrast, the lamellar regions provide higher strength and creep resistance due to their resistance to dislocation motion and crack propagation. By combining these two morphologies, the bimodal microstructure leverages the best features of both, offering an excellent compromise between ductility and strength, which is particularly valuable in aerospace and biomedical applications where both damage tolerance and load-bearing capacity are critical. Complete martensitic microstructure formation is the outcome of high alloy cooling rates above 410°C/s [26]. This microstructure is characterized by its exceptional hardness and strength. Recrystallization produces the equiaxed and bimodal microstructures. When β-grains slowly cool from the high temperature single-phase β region, into α+β grains, forming the lamellae microstructure [27, 18]. Mechanical properties such as ultimate tensile strength, yield strength and percentage elongation of Ti6Al4V alloy depends on the microstructures.

X-ray diffraction (XRD) analysis stands out as a non-destructive, sensitive technique for characterizing phase composition, residual stresses, and crystallographic texture in metallic materials. When combined with microstructural characterization methods such as optical microscopy and scanning electron microscopy (SEM), it provides perceptions into the internal architecture of LPBF-fabricated Ti6Al4V components [28, 29]. These combined techniques can provide detailed phase characterization of Ti6Al4V, making them essential tools in optimizing its microstructure and performance for aerospace applications [28]. This

study utilizes the optical and scanning electron microscopy, and XRD to investigate the various microstructural states of LPBF Ti6Al4V (ELI). The study reveals the presence of α′-martensite in the as-built condition and a gradual transformation to a more equilibrium α+β microstructure upon heat treatment.

2 Materials and methods

2.1 Production of test specimens

ASTM grade 23 gas atomized spherical Ti6Al4V (ELI) alloy powder was used to fabricate the samples for microstructural examination through a LPBF process. The powder was sourced from Germany's Bitterfeld-Wolfen-based TLS Technik GmbH. The EOSINT M290 machine (EOS GmbH, Munich, Germany) was used to produce the samples for use in this study, and the standard build layer thickness was 30 µm. The technical specification of the machine is presented in Table.1. Notably, the EOS M290 machine is equipped with pre-configured, optimized process parameters specifically designed for Ti6Al4V (ELI)

Table 1. EOS M290 Specifications

Build Volume	250 x 250 x 325 mm
Precision optics	F-theta lens; high-speed scanner
Power supply	32 A / 400 V
Power consumption	max. 8,5 kW / average 2,4 kW /with platform heating up to 3,2 kW
Compressed Air supply	7,000 hPa; 20 m³/h

A re-coater arm evenly distributed the powder around the build platform during the manufacturing process after loading it, and a laser beam then selectively scanned the powder. Using rotating strip patterns with a shift angle of 67° after each layer, specimens were created using a recurrent raster scanning technique. Cylindrical specimens with measurements of 6 mm in diameter and 80 mm in length shown in Figure 1 were fabricated.

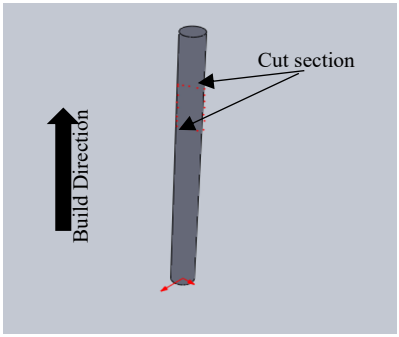

Fig. 1. Fabricated cylindrical test specimen with illustration of the cut section for microstructural analysis

2.2 Heat treatment of LPBF samples

The manufactured samples for microstructural and XRD analysis were divided into five groups, A, B, C, D, and E. Group A included as-built samples, whereas Group B included stress-relieved samples. Table 2 shows present details of Groups C, D, and E that were exposed to various heat treatment cycles after initially being stress relieved to reduce residual stress. The heat treatment was performed in a SuperSeries™ vacuum furnace system, model

SS12-24/13MX, to ensure controlled processing conditions. Following three hours of stress-relieving heat treatment at 650 °C, the furnace (FC) cools to room temperature.

Table 2. Post processing and cooling rates

Sample	**Heat treatment temperature (℃)**	**Cooling condition**	**Resident time (hours)**
Sample C	850	Furnace Cooling (FC)	2
Sample D	950	Rapid cooling of argon gas (FC)	2
Samples E	1100	Gas quench (FC)	2.5

2.3 Preparations of samples for microstructural and XRD analysis

The as-built samples (A) and heat-treated (B, C, D, and E) samples were sectioned along their build height for subsequent microstructural characterization. Each sample was cut into smaller pieces with a dimension of 9 mm in height, as illustrated in Figure 1 (red dotted line). The cutting was performed using a Leadwell T-7AM turn-mill machine, which has a clamping capacity of 200 mm and can accommodate workpieces up to 500 mm in length. The machine is equipped with a maximum spindle speed of 4500 rpm, ensuring precise sectioning of the samples without introducing excessive thermal or mechanical damage.

The small cylindrical samples were sectioned both longitudinally (along the build direction) and transversely (across the build direction) to enable comprehensive microstructural analysis. Electrical discharge machining (EDM) wire cutting was employed, providing high dimensional accuracy and preventing significant mechanical or thermal damage to the specimens.

2.4 Preparation of samples for microstructural analysis

Using the procedures presented in Table 3, the cut samples were mounted in MultiFast resin using a Struers Citopress-1 mounting machine.

Table 3. Procedure for mounting samples using MultiFast resin

Resin		Heating			Cooling		Total process time
	Quality (ml)	Time (min)	Temperature (℃)	Pressure (Bars)	Time (min)	Rate	Time (min)
MultiFast	25	3.5	180	250	2	High	5.5

After mounting, the samples were subjected to grinding and polishing following the protocol summarized in Table 4. The polished surfaces were first cleaned with tap water and dried using a stream of compressed air. Subsequently, the samples were cleaned for 15 minutes in an ultrasonic bath using ethanol as the cleaning solvent, then rinsed under running water and again dried with compressed air. To reveal the microstructural features, the cleaned surfaces were etched using Kroll's reagent, a weak aqueous solution consisting of 5 ml HNO_3, 10 ml HF (48% concentration), and 85 ml H_2O. Kroll's reagent is widely employed for etching titanium alloys to reveal their microstructural features, as it preferentially attacks the α and β phases, thereby enhancing the contrast between them and making the microstructural constituents clearly distinguishable under optical and electron microscopy.

Table 4. Protocol for grinding and polishing of Ti6Al4V samples.

Surface	Suspension	Lubricant	Time (min)
SiC Foil #220		Water	1:50
Largo	DiaP.All/Lar.9		5:00
Mol	DiaP.Mol3		2.20
MD-CHEM		Water	1:50

Subsequently, XRD analysis of the LPBF compressed samples was carried out using a PANalytical X'Pert Pro diffractometer equipped with a Cu-Kα radiation source (λ = 1.5406 Å). The operating conditions were set at 45 kV and 40 mA. Diffraction data were collected over an angular range of $35° \leq 2\theta \leq 70°$. This range was selected because it encompasses the most intense and well-defined diffraction peaks of Ti6Al4V, thereby allowing reliable identification of both the α/α′ and β phases. Within this range, the diffraction peaks corresponding to the α′/α-phase were identified at the $\{10\ \bar{1}0\}$, {0002}, $\{10\ \bar{1}1\}$, $\{10\ \bar{1}2\}$, $\{11\ \bar{2}0\}$, and $\{10\ \bar{2}3\}$ crystallographic planes, while the {110} reflection was assigned to the β-phase. These peaks were measured and analyzed in accordance with Bragg's law to evaluate the phase constitution and microstructural features of the samples.

3 Results and discussion

3.1 Microstructure of LPBF Ti6Al4V (ELI)

3.1.1 As built and stress relieved samples

In both the as-built and stress-relieved conditions, the microstructure of Ti6Al4V (ELI) fabricated by Laser Powder Bed Fusion (LPBF) predominantly consists of columnar prior β-grains aligned parallel to the build direction, as illustrated by the green lines shown in Figures 2(a) and 2(b). These β-grains contain fine acicular α′-martensite laths, a consequence of the extremely high cooling rates during solidification—often exceeding 10^6 °C/s [29, 30]. Such rapid thermal cycles promote a diffusionless transformation from β to α′, resulting in a non-equilibrium microstructure characterized by high internal stresses and limited ductility. Post-process stress-relief heat treatment, carried out at 650 °C for three hours, did not visibly alter the microstructure under optical microscopy or scanning electron microscopy (SEM), as seen in Figures 2(b) and 2(d). This observation is consistent with prior studies reported in [31, 32].

The columnar growth of prior β-grains is strongly influenced by the directional solidification associated with the LPBF process. Specifically, the steep thermal gradients that form within the melt pool—largely oriented perpendicular to the laser scanning direction and parallel to the build axis—govern grain orientation and morphology [33]. This results in anisotropic microstructures that can significantly impact mechanical properties, particularly in terms of tensile strength and fatigue resistance. While the as-built martensitic α′-phase contributes to increased hardness and strength, it may also introduce brittleness and reduced fracture toughness [34]. Therefore, tailoring heat treatment strategies is essential for balancing strength and ductility in LPBF Ti-6Al-4V components, especially for critical applications in aerospace and biomedical industries where mechanical performance and microstructural reliability are paramount.

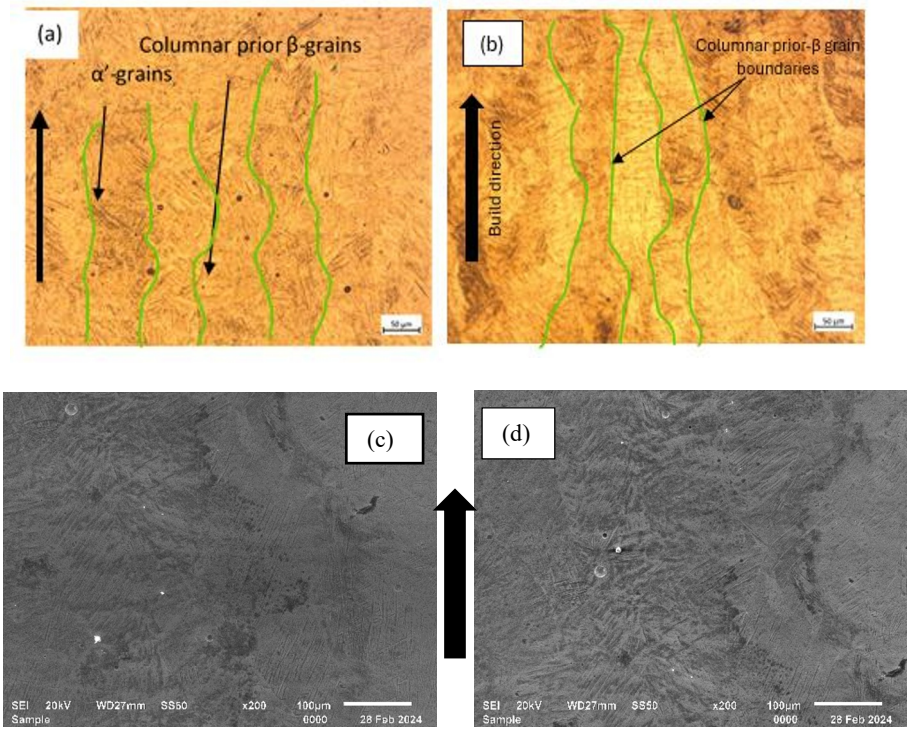

Fig. 2. Optical micrographs illustrating columnar prior-β-grains in (a) as-built, (b) stress-relieved samples under optical microscope and secondary electron images (SEI) (c) as-build, (d) stress relived samples in longitudinal view reference to the build orientation.

The transverse optical and scanning electron micrographs presented in Figures 3(a) and 3(b) reveal the presence of fine, needle-like α′-laths, commonly associated with a martensitic α′ microstructure. These features, highlighted within the green circles, are consistently observed in both the as-built and stress-relieved conditions.

Nevertheless, other investigations have demonstrated that the metastable α′ phase can undergo partial decomposition when subjected to prolonged heat treatment, even at sub-transus temperatures. Specifically, as noted in [32, 33], extended soaking at temperatures below 650 °C can promote the initiation of diffusional transformations, leading to the gradual evolution of the α′ martensite into equilibrium α + β phases. This transformation pathway is thermodynamically driven and can be critical in tailoring the final mechanical properties of the alloy by enhancing ductility and reducing residual stresses

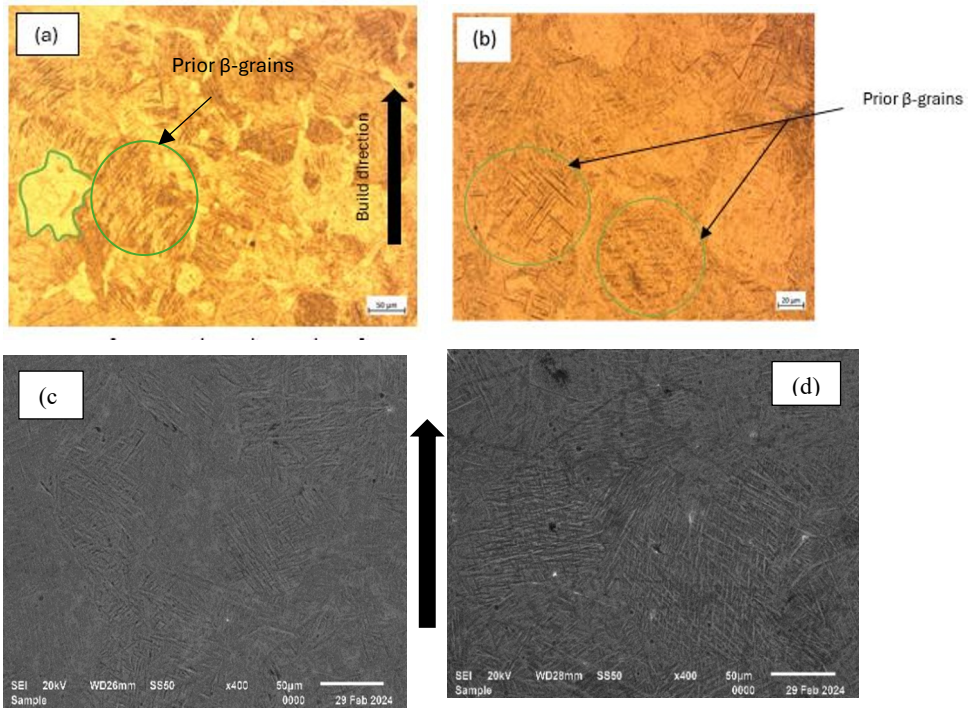

Fig. 3. Optical micrographs illustrating α' martensite microstructure for (a) as-build (b) stress relieved and SEIs (c) as-build, (d) stress relieved samples in transverse view in reference to the build orientation.

3.1.2 Heat treated microstructure of LPBF Ti6Al4V at 850℃, 950℃ and 1100 ℃

Samples C, D, and E underwent post-processing heat treatments at various temperatures, as specified in Table 2. Specifically, Sample C was subjected to a heat treatment at 850 °C for two hours, followed by furnace cooling. This treatment resulted in the transformation of the initial fine, acicular α′ martensitic microstructure into a more thermodynamically stable mixture of α and β phases. The α-phase appears as fine needle-like structures in the optical micrographs (Figure 4(a) and 4(c)), while under scanning electron microscopy (SEM), the α and β phases are distinguishable by their contrasting brightness—dark and bright regions, respectively, as seen in Figures 4(b) and 4(d).

Previous studies have confirmed that heat treatment temperatures exceeding 800 °C effectively decompose the metastable α′-martensite into the equilibrium α+β phase assemblage [34, 35]. The transformation kinetics and resulting phase distribution are strongly influenced by the martensite start temperature (Ms), which has been reported to vary between 575 °C and 800 °C for Ti6Al4V alloys [36, 21]. This variability in Ms is commonly attributed to several factors, including initial microstructural state, compositional homogeneity, and the presence of interstitial impurities such as oxygen, nitrogen, and carbon [24,26]. The initial microstructural effect on Ms in LPBF-fabricated components is particularly pronounced due to the high cooling rates and repetitive thermal cycling leading to formation of non-equilibrium α′ martensite. This can lead increase the value of Ms for metastable α′-martensite microstructure.

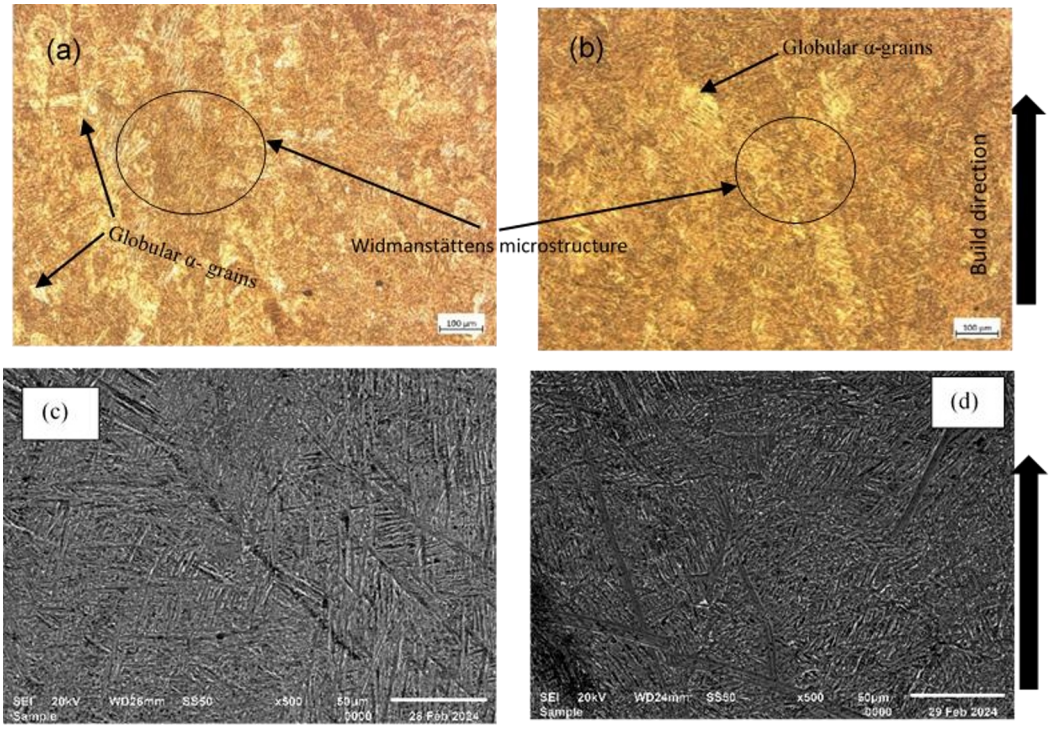

Fig. 4. (a) and (b) optical micrographs while (c) and (d) are SEIs of the same microstructure of heat-treated samples group C in longitudinal and transverse direction in reference the build direction, respectively**.**

The microstructure presented in Figure 4 exhibits a classical Widmanstätten pattern. The distinctive basket-weave microstructures are prominently observed in the higher-magnification SEI micrographs shown in Figures 4(c) and 4(d. As reported by Markovitz et al. [30], heat treatment of Ti6Al4V alloys within the temperature range of 800 °C to 850 °C promotes extensive martensitic decomposition, leading to the development of a microstructure characterized by an α+β lamellar morphology. Figure 5 depicts the typical microstructure of group D specimens that were subjected to heat treatment at 950 °C for 2 h, followed by rapid cooling under accelerated argon gas within the furnace chamber. The microstructure reveals prior β-grains containing α-laths, with the prior β-grain boundaries clearly delineated in Figures 5(c) and 5(d) under SEM. Furthermore, Figures 5(a) and 5(b) reveal regions of bimodal microstructure, which have been highlighted with red circles. Bimodal microstructures are generally reported to exhibit favourable combination of strength and ductility [18]. Areas exhibiting Widmanstätten morphology are indicated with green circles in both micrographs.

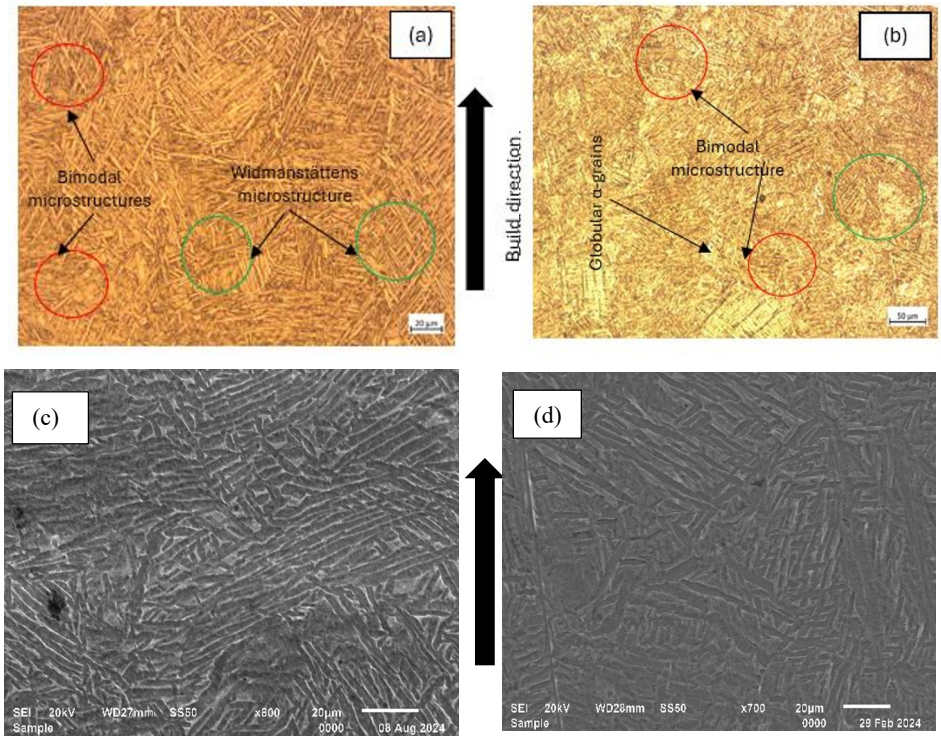

Fig. 5. Micrographs showing typical microstructures of sample group D (a) optical and (c) SEI in longitudinal view and (b) optical and (d) SEI in transverse direction in reference to the build direction.

The group E specimens were post processed at a temperature above the β-transus (1100 °C) for 2 h and 30 min, followed by rapid cooling in argon gas. The resulting microstructure is presented in Figure 6. This group is characterized by a typical basket-weave structure within large α colonies, indicative of significant grain growth, as highlighted by the green-circled regions. A clearer representation of this morphology is provided in Figures 6(c) and 6(d) at higher SEM magnifications. Similar microstructural features have been reported in previous studies [16, 18, 19, 31]. The applied heat treatment resulted in complete decomposition of α′ within the β-grains. Furthermore, the morphology illustrated in Figure 6 is characterized by equiaxed prior β-grains in both transverse and longitudinal sections, indicating the decomposition of the previously elongated columnar β-grains.

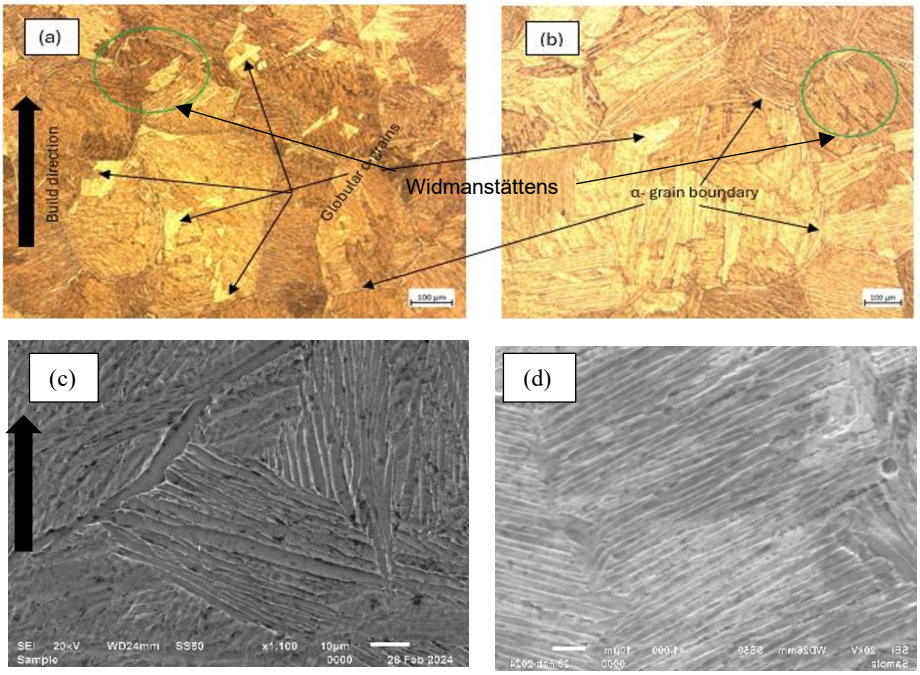

Fig. 6. Micrographs showing the microstructure of samples group E (a) optical micrograph, (c) SEI in longitudinal and (b) optical micrograph, (d) SEI in transverse direction reference the build direction.

3.2 XRD peak profiles of LPBF Ti6Al4V (ELI) parts

Figure 7 shows the XRD peak profiles for different forms of LPBF Ti6Al4V (ELI). The profiles indicate Braggs reflection of $\{10\bar{1}0\}, \{0002\}, \{10\bar{1}1\}, \{10\bar{1}2\}, \{11\bar{2}0\}$, *and* $\{10\bar{1}3\}$ the characteristic planes of the α′/α-phase, along with the {110} crystallographic plane of the β-phase. The {110} plane reflection is missing in sample A, B and C indicate absence of β-phase in these samples. Krakhmalev *et al* [28] and Muiruri *et al* [4] also reported similar observations on the XRD patterns of as-fabricated and stress-relieved samples. The difference in the peak profiles is observed in samples D, and samples E where the β-phase is observed in the pattern as these heat treatments were applied at temperature near the β-transus temperature.

Samples A and B display relatively low peak intensity, particularly around the angles of 35-39^{o} for position $\{10\bar{1}0\}$ and {0002} peaks corresponding to the primary α-phase. Broadening of peaks in sample A is observed and is attributed to high internal stresses, ultrafine grains, and a high density of crystallographic defects, which are typical features resulting from the rapid cooling rates inherent to the LPBF process.

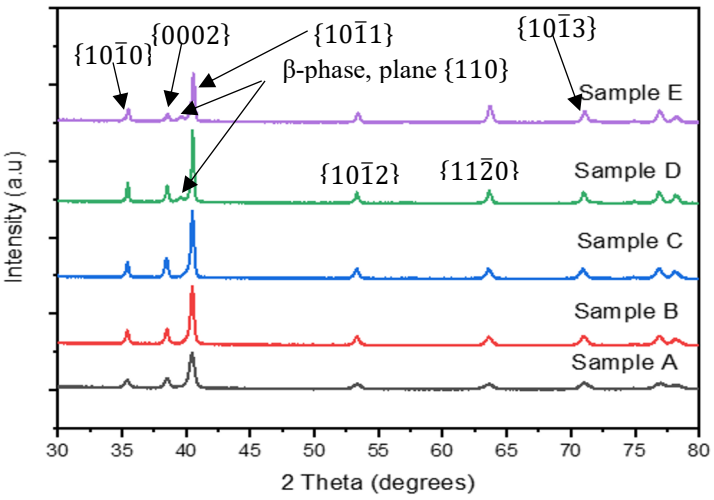

Fig. 7. XRD profile peak profiles of LPBF Ti6Al4V (ELI) in different forms.

The XRD patterns of samples A to E reveal a systematic evolution in the microstructural state of LPBF Ti6Al4V (ELI), as evidenced by the progressive narrowing, and intensity variation of key diffraction peaks.

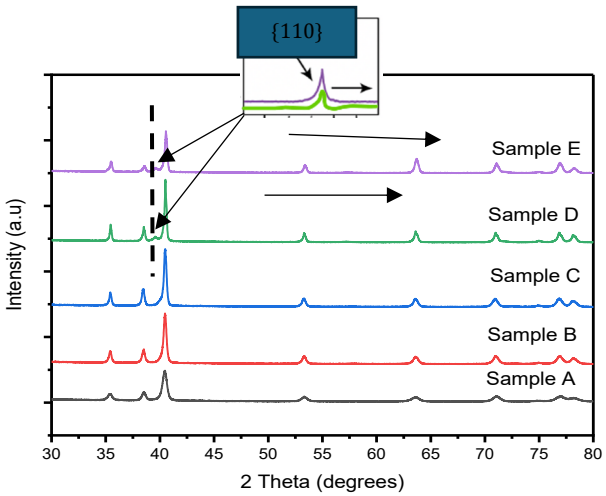

Fig. 8. Shifting of XRD peak profiles of LPBF Ti6Al4V (ELI) in Sample D and E.

The observed rightward shift in the α-phase peaks, particularly the (10$\bar{1}$0) and (0002) reflections (around 36–38°), in Sample D and Sample E indicates a reduction in interplanar spacing (d). According to Bragg's law, this shift toward higher 2θ values suggests that residual tensile strain present in the as-built sample (Sample A) is progressively relieved in subsequent samples via heat treatment. The distinct β-phase peak corresponding to the {110} plane clearly indicate that the phase is present in samples D and E. In sample A, B, and C conditions, this peak is absent due to rapid solidification of LPBF process. With adequate heat treatment, the β-phase is restored or stabilized, indicating reverse α′ → α and β transformation or retained β-phase growth. This transformation suggests diffusion-driven

phase kinetics, enhanced by thermal exposure during post-processing. Following the application of a stress-relief heat treatment, the diffraction peaks become noticeably sharper and more defined, accompanied by minor shifts toward lower 2θ values of 35 to 40°as illustrated in figure 7 (sample B).

With the progressive heat treatments (samples B, C, and D), the diffraction patterns exhibit further peak sharpening and increased intensity of the α-phase reflections. This narrowing of diffraction peaks is consistence with grain coarsening and reduction in micro-strain. Additionally, the gradual enhancement of α-phase peak intensity, particularly in samples C and samples D, implies a growth in the equilibrium α-phase volume fraction, consistent with phase stabilization during heat treatment. A reduction in peak intensity in samples E is due to changes in phase distribution resulting from thermal post-processing. The evolution of the microstructure, including grain growth and potential increase in β-phase content, leads to decreased diffracted intensity from the α-phase planes. Additionally, any loss of preferred orientation or increased surface scattering may further reduce the measured peak intensities. This microstructural coarsening and phase stabilization are essential for improving the mechanical properties required for aerospace and other critical structural applications, providing enhanced ductility, thermal stability, and fatigue performance [23, 32].

The XRD results demonstrate a clear evolution from a highly strained, martensitic-dominated microstructure in the as-built state to a stable, coarse-grained α + β dual-phase structure after successive heat treatments. These findings highlight the critical role of post-processing heat treatments in tailoring the microstructural of LPBF Ti6Al4V (ELI) components for demanding applications.

4 Conclusion

The study aimed at analysing microstructures and XRD peak profiles of different forms of LPBF Ti6Al4V alloy. The following conclusions were derived from the study.

- The stress-relieving heat treatment of LPBF Ti-6Al-4V does not appear to significantly transform the acicular α′ martensitic microstructure observed in the as-built condition, as confirmed by both optical microscopy and scanning electron microscopy. While stress relief effectively reduces residual stresses generated during rapid solidification, the relatively low temperatures employed in this treatment are insufficient to drive substantial phase transformation or breakdown of α′ into the steadier α+β phases. As a result, the needle-like morphology of the as-built microstructure remains largely unchanged.
- At high temperature heat treatment, the α’ laths are replaced by α-and β-laths
- No β-stage was detected in the as-built or stress-relieved LPBF Ti-6Al-4V (ELI) samples, as confirmed by the XRD data obtained in this study. The presence of the β-phase was confirmed in both group D and group E samples of the LPBF Ti6Al4V alloy.

The future works aims at analysing the dislocation densities of LPBF Ti6Al4V (ELI) at different level of strain using the XRD and scanning electron microscopy. This will be accomplished using a combination of XRD for quantitative defect characterization and SEM for direct microstructural observation. The objective is to establish a correlation between dislocation density, strain hardening behaviour, and the resulting mechanical performance of the alloy. Such insights are expected to contribute to improved process optimization and

predictive modelling for structural components in the aerospace sector, where high strength, fatigue resistance, and reliability are critical.

References

[1] T. Campbell, C. Williams, O. Ivanova and B. Garrett, "Could 3D printing change the world," *echnologies, Potential, and Implications of Additive Manufacturing, Atlantic Council, Washington, DC,* **3**, no. 1, p. 18, (2011).

[2] R. R. Boyer , "An overview on the use of titanium in the aerospace industry," *Materials Science and Engineering,* **1-2**, pp. 103-114, (1996).

[3] B. Dutta and S. F. Froes, "The additive manufacturing (AM) of titanium alloys," *Metal powder report,* **72**, no. 2, pp. 96-106, (2017).

[4] I. Gibson , D. W. Rosen and B. Stucker, Additive manufacturing technologies 3D printing, rapid prototyping, and direct digital manufacturing, New York : Springer , (2015).

[5] A. Muiruri, M. Maringa and W. du Preez, "X-ray diffraction profile analysis of martensitic Ti6Al4V (ELI) parts produced by laser powder bed fusion," in *MATEC Web of Conferences*, (2023).

[6] A. Muiruri , M. Maringa and W. du Preez, "Evaluation of dislocation densities in various microstructures of additively manufactured Ti6Al4V (ELI) by the method of x-ray diffraction," *Materials,***13**, no. 23, p. 5355, (2020).

[7] L. F. Monaheng , W. B. du Preez, N. Kotze and M. Vermeulen , "Topology optimisation of an aircraft nose-wheel fork for production in Ti6Al4V by the Aeroswift high-speed laser powder bed fusion machine," *In MATEC Web of Conferences,* **321**, p. 03013, (2020).

[8] C. Leyens and M. Peters, Titanium and titanium alloys, New York: CRC Press, (2006).

[9] F. H. Froes, R. Boyer and B. Dutta, "ADDITIVE MANUFACTURING FOR AEROSPACE APPLICATIONS--Part I: Fabrication of aerospace components using additive manufacturing has matured to the point where part microstructures and mechanical properties compare well with those of conventionally produced ma," *Advanced Materials & Processes,***175**, no. 5, pp. 36-41, (2017).

[10] T. G. Kulkami and N. Bhattacharya, "Use of titanium and its alloy in aerospace and aircraft industries," *Int. J. Creat. Res. Thoughts,* **8**, pp. 1383-1396, (2020).

[11] A. Gomez-Gallegos, P. Mandal, D. Gonzalez, N. Zuelli and P. Blackwell, "Studies on titanium alloys for aerospace application," *In Defect and Diffusion Forum,* **385**, pp. 419-423, (2018).

[12] I. Inagaki, T. Takechi, Y. Shirai and N. Ariyasu, "Application and features of titanium for the aerospace industry," *Nippon steel & sumitomo metal technical report,* **106**, no. 106, pp. 22-27, (2014).

[13] J. C. Williams and R. R. Boyer , "Opportunities and issues in the application of titanium alloys for aerospace components.," *Metals,* **10**, no. 6, p. 705, (2020).

[14] K. Yamanaka, A. Kuronda, M. Ito, M. Mori, H. Bian, T. Shobu, S. Sato and A. Chiba, "Quantifying the dislocation structures of additively manufactured Ti–6Al–4V alloys using X-ray diffraction line profile analysis," *Additive Manufacturing,* **37**, p. 101678, (2021).

[15] D. Herzog, V. Seyda, E. Wycisk and C. Emmelmann, "Additive manufacturing of metals," *Acta Materialia,* **117**, pp. 371-392, (2016).

[16] B. Vracken , L. Thijs, J.-O. Kruth and J. Van Humbeeck, "Heat treatment of Ti6Al4V produced by Selective Laser Melting: Microstructure and mechanical properties," *Journal of Alloys and Compounds,* **541**, pp. 177-185, (2012).

[17] M. G. Moletsane , Microstructure and mechanical properties of Ti6Al4V (ELI) parts produced by DMLS (Masters dissertation, Bloemfontein, Bloemfontein : Central University of Technology, Free State, (2016).

[18] A. A. Antonysamy, Microstructure, texture and mechanical property evolution during additive manufacturing of Ti6Al4V alloy for aerospace applications, Manchestser: The University of Manchester (United Kingdom)., (2012).

[19] A. Muiruri, Investigation of the High Strain Rate Behaviour and Impact Toughness of Ti6Al4V (ELI) Parts Built by the EOS M280 DMLS System with Standard Process Parameters; As-Built and Stress Relieved, Bloemfontein: Department of Mechanical and Mechatronics Engineering, (2018).

[20] T. Moloi, T. C. Dzogbewu, M. Maringa and A. Muiruri, "The Effect of Temperature on the Microstructures of Additively Manufactured Ti6Al4V (Eli)," *Iranian Journal of Materials Science & Engineering,* **21,** no. 3, (2024).

[21] R. Pederson, "Microstructure and phase transformation of Ti-6Al-4V," Luleå tekniska universitet, Luleå, (2002).

[22] D. Zöllner, "Impact of a strong temperature gradient on grain growth in films," *Modelling and Simulation in Materials Science and Engineering,* **30**, no. 2, p. 025010, (2022).

[23] F. C. Campbell, Fatigue and fracture: understanding the basics, ASM International , (2012).

[24] J. R. Zhao, F. Y. Hung, T. S. Lui and Y. L. Wu, "The relationship of fracture mechanism between high temperature tensile mechanical properties and particle erosion resistance of selective laser melting Ti-6Al-4V alloy," *Metals,* **9**, no. 5, p. 501, (2019).

[25] J. Song, Y. Han, M. Fang, F. Hu, L. Ke, Y. Li, L. Lei and W. Lu, "Temperature sensitivity of mechanical properties and microstructure during moderate temperature deformation of selective laser melted Ti-6Al-4V alloy," *Materials Characterization,* **165**, p. 110342, (2020).

[26] S. Liu and Y. C. Shin, "Additive manufacturing of Ti6Al4V alloy: A review.," *Materials and Design,* **164**, p. 107552, (2019).

[27] J. Sieniawski, W. Ziaja, K. Kubiak and M. Motyka, "Microstructure and mechanical properties of high strength two-phase titanium alloys," *Titanium alloys-advances in properties control ,* pp. 69-80, (2013).

[28] G. P. Konda, S. Kolla and J. Eckert, "Additive manufacturing processes: Selective laser melting, electron beam melting and binder jetting—Selection guidelines," *Materials ,* **10**, no. 6, p. 672, (2017).

[29] P. M. Lekoadi, M. Tlotleng, N. Maledi and B. N. Masina, "Improving the microstructure of high speed selective laser melted Ti6A14V components by varying residence time during heat treatment," in *RAPDASA conference*, Bloemfontein, (2019).

[30] P. Krakhmalev, G. Fredriksson, I. Yadroitsava, N. Kazantseva, A. Du Plessis and I. Yadroitsev, "Deformation behavior and microstructure of Ti6Al4V manufactured by SLM," *Physics Procedia,* **83**, pp. 778-788, (2016).

[31] G. M. Ter Haar and T. H. Becker, "Low temperature stress relief and martensitic decomposition in selective laser melting produced Ti6Al4V," *Material Design & Processing Communications,* **3**, no. 1, p. e138, (2021).

[32] D. D. Malka-Markovitz, A. Katsman, A. Shirizly and M. Bamberger, "Microstructure and mechanical properties of heat treated selective laser melting manufactured Ti-6Al-4V.," *J. Int. Sci. Publ. Mater. Methods Technol.(Online),* **10**, pp. 495-505, (2016).

[33] T. Ahmed and H. J. Rack , "Phase transformations during cooling in α+ β titanium alloys," *Materials Science and Engineering:,* **243**, no. 1-2, pp. 206-211, (1998).

[34] H. Jaber , J. Kónya, K. Kulcsár and T. Kovács, "Effects of annealing and solution treatments on the microstructure and mechanical properties of Ti6Al4V manufactured by selective laser melting," *Materials,* **15**, no. 5, p. 1978, (2022).

[35] G. Lütjering and J. C. Williams, Titanium matrix composites, Berlin Heidelberg: Springer, 2007, pp. 367-382.

[36] P. J. Withers and H. K. Bhadeshia, "Residual stress. Part 1–measurement techniques," *Materials science and Technology,* **17**, no. 4, pp. 355-365, (2001).

[37] H. Qianli, X. Liu, X. Yang, R. Zhang, Z. Shen and Q. Feng, "Specific heat treatment of selective laser melted Ti–6Al–4V for biomedical applications," *Frontiers of Materials Science ,* **9**, pp. 373-381, (2015).

[38] T. Vilaro , C. Colin and J. D. Bartout, "As-fabricated and heat-treated microstructures of the Ti-6Al-4V alloy processed by selective laser melting," *Metallurgical and materials transactions A,* **42**, no. 10, pp. 3190-3199, (2011).